Observation of Decrease of Supercurrent in the Gapless Region

O. P. HANSEN
Physics Laboratory I, H. C. Ørsted Institute, University of Copenhagen, Copenhagen, Denmark
(Received 23 October 1968; revised manuscript received 6 February 1969)

The dependence of superfluid current density J on superfluid velocity v was measured in a hollow superconducting cylinder of indium placed in an axial low-frequency magnetic field. In order to enter the v region for which a decrease of J as a function of v is predicted, the interior of the cylinder was filled with a superconducting rod. The measured quantities were the flux ϕ_J arising from J and the magnitude H_e of the low-frequency magnetic field which is related to v. The experimental results are graphs showing ϕ_J as a function of H_e. At temperatures close to the transition temperature of the film, the ϕ_J-H_e graphs were linear for small H_e, whereas for larger H_e, a maximum in ϕ_J followed by a decrease was clearly observed. The temperature dependence and the maximum value of ϕ_J were found—within experimental accuracy—to be in agreement with the predictions of the Ginzburg-Landau theory.

I. INTRODUCTION

ONE of the basic properties of a superconductor is that it can carry an electric current with the total absence of resistance. It is consequently of interest to investigate the factors which limit the magnitude of the supercurrent and the circumstances under which it disappears. The nature of the experimental conditions is of importance in such an investigation. Very often the superconductor is connected through electrical leads to an external network, and a current, determined by this network, is passed through the superconductor. By increasing the current until a voltage across the superconductor appears, the so-called critical current is found. This kind of experiment, though useful in a number of investigations, has the disadvantage that the supercurrent is controlled by the external network. To avoid this disadvantage, the superconductor should not be simply connected, but rather should be in the form of, say, a hollow cylinder, in which the velocity of the superconducting electron pairs (the superfluid velocity) is determined by inductive coupling with an axial variable magnetic field H_e. In such an experiment, the supercurrent is allowed to adjust itself freely. The magnitude of the supercurrent can be found by measuring the flux ϕ_J which arises from the supercurrent. The experiment to be described in this paper is of the latter kind. The experimental results are graphs showing ϕ_J as a function of H_e.

In the London equations of superconductors,[1] the relation between the supercurrent and the vector potential of the magnetic field is linear, the coefficient of proportionality being a function of temperature only. A phenomenological theory which is not restricted to a linear dependence of supercurrent on vector potential was given by Ginzburg and Landau (GL).[2] They introduced the so-called order parameter Ψ which depends on temperature, position, and vector potential. Under conditions which we shall discuss in Sec. II the relation between supercurrent density $\mathbf{J}$ and vector potential $\mathbf{A}$ is

$$(4\pi/c)\mathbf{J}=-(f^2/\lambda^2)\mathbf{A}, \tag{1}$$

where $f=|\Psi(\mathbf{r},T,\mathbf{A})/\Psi(\mathbf{r},T,0)|$, $\mathbf{r}$ represents the spatial position, and λ is the penetration depth. As f^2 is proportional to the density of superconducting electron pairs, we see from (1) that $\mathbf{A}$ is proportional to the superfluid velocity. In Sec. II we shall find that f is a decreasing function of A and becomes zero for sufficiently large A. This means that J as a function of A has a maximum followed by a decrease to zero.

The microscopic interpretation of the maximum and the following decrease in supercurrent, predicted by (1), has been discussed by several authors[3–5] on the basis of the theory of Bardeen, Cooper, and Schrieffer.[6] According to this interpretation, the gap in the excitation spectrum disappears when the superfluid velocity is larger than the so-called depairing velocity. (For a clean superconductor this equals Δ/p_F, where Δ is the pair potential and p_F is the Fermi momentum.) The depairing velocity is roughly coincident with the velocity at which the supercurrent attains its maximum, and so over the maximum there is a (gapless) region where the gap is zero. Although there is no gap, the superconductor retains its infinite conductivity.[7]

In the first experiments on a nonlinear relation between J and A, the predicted decrease in supercurrent was not observed.[8–11] In the tunneling measurements,[9,11] the maximum in supercurrent was not reached, and in the low-frequency induction measurements[8] and the microwave transmission measurements,[10] disturbing effects in the region near the maximum made a compari-

[1] F. London, *Superfluids* (Wiley-Interscience, Inc., New York, 1950, or Dover Publications, Inc., New York, 1961), Vol. I.
[2] V. L. Ginzburg and L. D. Landau, Zh. Eksperim. i Teor. Fiz. **20**, 1064 (1950).
[3] J. Bardeen, Rev. Mod. Phys. **34**, 667 (1962).
[4] K. T. Rogers, Ph.D. thesis, University of Illinois, 1960 (unpublished).
[5] R. H. Parmenter, RCA Rev. **23**, 323 (1962).
[6] J. Bardeen, L. N. Cooper, and J. R. Schrieffer, Phys. Rev. **108**, 1175 (1957).
[7] E. Brun Hansen, Physica **39**, 271 (1968).
[8] C. D. Mitescu, Rev. Mod. Phys. **36**, 305 (1964).
[9] J. L. Levine, Phys. Rev. Letters **15**, 154 (1965).
[10] K. Rose and M. D. Sherrill, Phys. Rev. **145**, 179 (1966).
[11] C. D. Mitescu, in *Proceedings of the Tenth International Conference on Low-Temperature Physics, Moscow, 1966*, edited by M. P. Malkov (Proizvodstrenno-Izdatel'skii Kombinat, VINITI, Moscow, 1967), Vol. 2B, p. 366.

son with (1) difficult. We have recently reported an observation of decreasing J in an experiment using cylindrical geometry and an axial low-frequency magnetic field.[12] Another experiment in which such a decrease was observed has been reported by Bhatnagar and Stern[13]; they employed a sandwich geometry and a different experimental technique. In the present paper we shall describe the details of the experiment reported in Ref. 12. The sample was an In cylinder, and following the proposal of Fulde and Ferrell,[14] the interior of this was filled with a superconducting rod in order to enter the gapless region. The thickness of the In cylinder was small compared with the coherence length, and accordingly the order parameter was assumed to be independent of position.

A discussion of why it is necessary to fill the interior of the cylinder with a superconducting rod in order to enter the gapless region will be given in Sec. II, along with the formulas used in the interpretation of the experimental results. The basis of this interpretation is the GL theory. The experimental technique will be described in Sec. III and the experimental results in Sec. IV. Section V contains a discussion of the results. The conclusion will be given in Sec. VI.

II. GL THEORY FOR A THIN SUPERCONDUCTING CYLINDER

A. GL Equations

The GL theory for a thin hollow superconducting cylinder has been discussed in detail by Douglass,[15] and the discussion given below follows his method, but includes the changes due to the presence of a superconducting rod in the interior of the cylinder. The GL equations relate the order parameter Ψ to the vector potential $\mathbf{A}$ through a pair of coupled nonlinear differential equations. For a cylinder of arbitrary cross section, with an external field H_e parallel to the axis, the GL equations can be expressed in the form[2]

$$[\nabla+(ie^*/\hbar c)\mathbf{A}]^2\psi+(\kappa^2/\lambda^2)(1-|\psi|^2)\psi=0, \quad (2)$$

$$\nabla\times\nabla\times\mathbf{A}=(i\hbar c/2e^*\lambda^2)(\psi^*\nabla\psi-\psi\nabla\psi^*)-(|\psi|^2/\lambda^2)\mathbf{A}, \quad (3)$$

where $\psi=\Psi(\mathbf{r},T,\mathbf{A})/\Psi(\mathbf{r},T,0)$, and $e^*=2e$ is the charge of a "Cooper pair."[16] The penetration depth λ and the dimensionless coupling constant κ are given by[17]

$$\lambda^2=\lambda_L^2/\chi=mc^2/4\pi e^{*2}|\Psi(T,0)|^2\chi, \quad (4)$$

$$\kappa=\kappa_0/\chi=\sqrt{2}e^*\lambda_L^2H_{cb}/\hbar c\chi=\sqrt{2}e^*\lambda^2H_{cb}/\hbar c, \quad (5)$$

where H_{cb} is the bulk critical field, and χ is a function of the ratio of the bulk coherence length ξ_0 to the electronic mean free path l; χ can be approximated[18] within an accuracy of about 20% by

$$\chi=(1+\xi_0/l)^{-1}. \quad (6)$$

The supercurrent density $\mathbf{J}$ as given from Maxwell equations is

$$(4\pi/c)\mathbf{J}=\nabla\times\nabla\times\mathbf{A}, \quad (7)$$

which, with the use of (3), can be written

$$(4\pi/c)\mathbf{J}=(i\hbar c/2e^*\lambda^2)(\psi^*\nabla\psi-\psi\nabla\psi^*)-(|\psi|^2/\lambda^2)\mathbf{A}. \quad (8)$$

Taking advantage of the cylindrical geometry used in the present experiment, we shall assume that A is a function only of radial distance r and we shall choose the following gauge for A:

$$A(r)=\phi(r)/2\pi r, \quad (9)$$

where $\phi(r)$ is the magnetic flux through an area bounded by a circle of radius r. The gauge chosen for A determines the phase of ψ. The choice represented by (9) gives

$$\psi=fe^{-i\nu\theta}, \quad (10)$$

where θ is the cylindrical angle and ν is the fluxoid quantum number. If the fluxoid is zero, then ψ is real, and we get Eq. (1) for the relation between $\mathbf{J}$ and $\mathbf{A}$.

In the following, we shall assume throughout that the fluxoid is zero and, moreover, that f is independent of position. The justification—in the experiment to be described—for these assumptions will be discussed in Secs. III and IV. The method used when solving (2) and (3) is to find $A(r)$ from (3) with relevant boundary conditions. After that, a self-consistent solution for f is obtained directly from (2):

$$f^2=1-(\lambda e^*/\kappa\hbar c)^2\langle A(r)^2\rangle_{\mathrm{av}}, \quad (11)$$

where an average over the superconductor has been substituted for the spatially varying terms. The spatial average of a quantity O is defined as

$$\langle O\rangle_{\mathrm{av}}=\frac{2}{(r_1+d)^2-r_1^2}\int_{r_1}^{r_1+d} rO(r)dr, \quad (12)$$

where r_1 is the inner radius of the superconducting cylinder and d is the thickness of its wall [cf. Fig. 2(a)].

B. Significance of the Superconducting Rod

Before the application of the method mentioned above, we shall discuss why it is necessary to fill the interior of the superconducting cylinder with a superconducting rod in order to enter the gapless region. The arguments are the same as those given by Fulde and Ferrell.[14] We start by considering the case of a hollow superconducting cylinder with *no superconducting rod*

[12] O. P. Hansen, in *Abstracts of the Eleventh International Conference on Low-Temperature Physics, St. Andrews, 1968* (The University of St. Andrews, St. Andrews, 1968), Sec. B3.10.

[13] A. K. Bhatnagar and E. A. Stern, Phys. Rev. Letters **21**, 1061 (1968).

[14] P. Fulde and R. A. Ferrell, Phys. Rev. **131**, 2457 (1963).

[15] D. H. Douglass, Jr., Phys. Rev. **132**, 513 (1963).

[16] L. N. Cooper, Phys. Rev. **104**, 1189 (1956).

[17] L. P. Gor'kov, Zh. Eksperim. i Teor. Fiz. **37**, 1407 (1959) [English transl.: Soviet Phys.—JETP **10**, 998 (1959)].

[18] D. H. Douglass, Jr., Phys. Rev. **124**, 735 (1961).

inside, and we assume that $r_1 \gg d$ and $d \ll \lambda$. Because of the assumption $r_1 \gg d$, we may neglect the flux in the wall of the superconducting cylinder when compared to $\phi(r_1)$, and for the vector potential in the wall use $A(r_1)$. The assumption $d \ll \lambda$ means that in the wall J and A are independent of position. We then get from (1) and (11)

$$-(4\pi/c)J=(1/\lambda^2)[1-(\lambda e^*/\kappa\hbar c)^2 A(r_1)^2]A(r_1). \quad (13)$$

This relation is sketched in Fig. 1. However, (13) does not relate J to the external magnetic field. $A(r_1)$ is not simply the vector potential of the external field, but contains an additional term due to the magnetic field set up by J. Thus,

$$A(r_1)=A_e(r_1)+A_J(r_1), \quad (14)$$

where A_e is the vector potential of the external field and A_J is that due to J. For $A_J(r_1)$ we write, according to (9),

$$A_J(r_1)=(4\pi/c)dJ\pi r_1^2/2\pi r_1. \quad (15)$$

We then get from (14)

$$-(4\pi/c)J=-(2/r_1 d)A(r_1)+(2/r_1 d)A_e(r_1). \quad (16)$$

In Fig. 1, this relation is represented by a straight line ("load line"). Solutions of (13) and (16) are obtained as the intersection of the "current characteristic" (13) with the load line (16). (If there are two intersections, then only the one with smallest abscissa represents a stable solution.) The effect of increasing the external field can be visualized as a parallel translation of the load line so that its intersection with the abscissa axis is shifted continuously to larger values. Clearly, to explore the entire current characteristic it is necessary that the slope of the load line is larger than or equal to the maximum slope of the current characteristic. The latter quantity is found from (13) to be $-2/\lambda^2$, and to explore the entire current characteristic it is thus necessary that

$$r_1 d/\lambda^2 \lesssim 1. \quad (17)$$

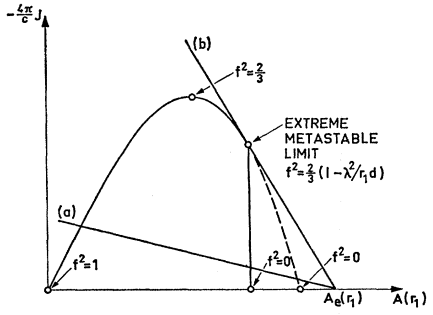

FIG. 1. Current characteristic and two load lines (a) and (b). J is the supercurrent density; $A(r_1)$ is the vector potential at radial distance r_1; A_e is the vector potential of external magnetic field; f is the magnitude of reduced order parameter. The intersection between one of the load lines and the current characteristic determines the actual $A(r_1)$ and $-4\pi J/c$ for an applied A_e. With a flat load line (a) the maximum in the current characteristic is almost coincident with the "extreme metastable limit," and the region of decreasing J is inaccessible. The steeper load line (b) is drawn corresponding to the extreme metastable limit being reached.

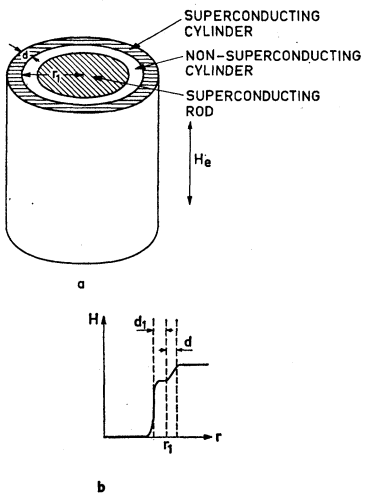

FIG. 2. (a) Model of the sample. H_e is the external low-frequency magnetic field; r_1 is the inner radius of the superconducting cylinder; d is the thickness of the wall of the superconducting cylinder. (b) Dependence of magnetic field H on radial distance r.

When this condition is fulfilled, we should expect J to go continously to zero as A_e is increased. If $r_1 d/\lambda^2$ is larger than unity, then by increasing A_e, the load line will let the current characteristic go at the point where the slope of this equals that of the load line [cf. Fig. 1, load line (b)]. The corresponding value of f^2 is found to be

$$f^2=\tfrac{2}{3}(1-\lambda^2/r_1 d). \quad (18)$$

This point on the current characteristic represents the so-called "extreme metastable limit." At this, J is expected to drop discontinuously to zero. For a more extensive discussion of the extreme metastable limit the reader is referred to the paper by Douglass.[15] Here we shall only mention that at $f^2=0$, the fluxoid is expected to adjust itself and J is expected to start rising again, repeating its previous graph until the critical field is reached.

For a hollow cylinder, the fulfillment of (17) requires an almost impossible small radius. As pointed out by Fulde and Ferrell,[14] this is due to the relatively large self-inductance of the cylinder. [We see from (15) and (16) that the slope of the load line is inversely proportional to the self-inductance.] The self-inductance can be decreased by filling the interior of the cylinder with a superconducting rod. Because of the Meissner effect, there will be no magnetic flux lines in this rod, except for a surface layer of thickness approximately equal to the penetration depth of the rod material. In order that the superconductivity in the rod does not influence that in the cylinder, the rod should be separated from the cylinder by a nonsuperconducting material. The final sample model is shown in Fig. 2(a). The dependence of magnetic field on radial distance is sketched in Fig. 2(b).

We shall now look upon the load-line argument for the sample model in Fig. 2(a). The flux $\phi(r_1)$ is

$$\phi(r_1)=\int_0^{r_1} 2\pi r H(r)dr, \tag{19}$$

and we introduce new quantities d_1 and H_i defined by the relations

$$H_i=H_e+(4\pi/c)dJ, \tag{20}$$

$$\phi(r_1)=2\pi r_1 d_1 H_i, \tag{21}$$

where H_e is the external magnetic field and r_1 is assumed to be much larger than d_1. The value of $\phi(r_1)$ as given by (21) is $2d_1/r_1$ times that for a hollow cylinder with no superconducting rod inside. This means that—unless d_1 is much larger than d—we can no longer neglect the flux in the wall of the cylinder and use $A(r_1)$ for the vector potential in it. But, if we assume that $d_1 \gg d$, then the argumentation will be as before. The slope of the load line will be $-1/d_1 d$, and instead of (17) we get

$$2dd_1/\lambda^2 \leqslant 1, \tag{22}$$

which is more easy to fulfill than (17).

C. Solution of GL Equations

The load-line discussion given above was based on assumptions which were not justified in the experiment to be described, namely, the assumptions that $d \ll \lambda$ and $d \ll d_1$. In the following, we shall skip these assumptions but still assume that $r_1 \gg d_1$, $r_1 \gg d$, f is independent of position, and the fluxoid is equal to zero.

The relation between J and H_e will now be established via the boundary conditions for the sample model in Fig. 2(a). These boundary conditions are

$$\nabla \times \mathbf{A}=\mathbf{H}_e, \quad \text{for } r=r_1+d \tag{23}$$

$$A/d_1=|\nabla \times \mathbf{A}|, \quad \text{for } r=r_1 \tag{24}$$

where the last condition is found by noting that $A(r_1)=d_1 H_i$ according to (9) and (21). In the results given below, series expansions of hyperbolic functions with argument df/λ have been used. The justification for this approximation will be discussed in Sec. V. For details concerning the solution, the reader is referred to the Appendix.

The average value of the vector potential in the wall of the cylinder is found from (3), (23), (24), and (12) to be

$$\langle A\rangle_{\text{av}}=d_1 H_e \frac{1+d/2d_1}{1+\frac{1}{2}(1+d/2d_1)\gamma^2 f^2}, \tag{25}$$

where

$$\gamma^2=2dd_1/\lambda^2. \tag{26}$$

From (11) and (12) we find

$$f^2=1-\frac{(d_1 H_e/\sqrt{2}\lambda H_{cb})^2[1+d(1+d/3d_1)/d_1]}{[1+\frac{1}{2}(1+d/2d_1)\gamma^2 f^2]^2}. \tag{27}$$

When the value of $\langle A\rangle_{\text{av}}$ is inserted into (1), we get for the average current density

$$\frac{4\pi d}{c}\langle J\rangle_{\text{av}}=\frac{\frac{1}{2}\gamma^2 f^2(1+d/2d_1)}{1+\frac{1}{2}(1+d/2d_1)\gamma^2 f^2}H_e. \tag{28}$$

Another useful expression for $\langle J\rangle_{\text{av}}$ is found by elimination of H_e from (27) and (28); this gives[19]

$$|\langle J\rangle_{\text{av}}|=\frac{cH_{cb}}{2\pi\sqrt{2}\lambda}\frac{1+d/2d_1}{[1+d(1+d/3d_1)/d_1]^{1/2}}f^2(1-f^2)^{1/2}. \tag{29}$$

From this equation we find that $|\langle J\rangle_{\text{av}}|$ has a maximum at $f^2=\frac{2}{3}$, and that the maximum value is

$$|\langle J\rangle_{\text{av}}|_{\max}=\frac{(8/27)^{1/2}cH_{cb}}{4\pi\lambda}\frac{1+d/2d_1}{[1+d(1+d/3d_1)/d_1]^{1/2}}. \tag{30}$$

The corresponding value of the external field is found from (27):

$$|H_{2/3}|=\frac{(\frac{2}{3})^{1/2}\lambda H_{cb}}{d_1}\frac{1+\frac{1}{3}(1+d/2d_1)\gamma^2}{[1+d(1+d/3d_1)/d_1]^{1/2}}. \tag{31}$$

For $f^2=0$ we find from (27) that $H_0=H_e$:

$$|H_0|=(\sqrt{2}\lambda H_{cb}/d_1)[1+d(1+d/3d_1)/d_1]^{-1/2}. \tag{32}$$

Moreover, in the interpretation of the experimental results we shall use the derivative $d\langle J\rangle_{\text{av}}/dH_e$ for small H_e. From (28) we find, for $H_e \to 0$, that

$$\frac{d\langle J\rangle_{\text{av}}}{dH_e}=-\frac{c}{4\pi d}\frac{1+d/2d_1}{1+d/2d_1+2/\gamma^2}. \tag{33}$$

Finally, we should bear in mind that the presented formulas are valid only as long as the fluxoid is zero, and therefore they cannot be used for values of H_e larger than H_0. If H_e is increased beyond this value, we finally reach the film critical field H_c which, for $d/\lambda<\sqrt{5}$, is given by[20]

$$H_c=2(\sqrt{6})\lambda H_{cb}/d. \tag{34}$$

We see from (32) and (34) that

$$|H_0|/H_c=(d/2\sqrt{3}d_1)[1+d(1+d/3d_1)/d_1]^{-1/2}. \tag{35}$$

The right-hand side of this equation is found to be less than $\frac{1}{2}$ for all values of d/d_1. This means that the value of H_c is at least twice the value of H_0.

III. EXPERIMENTAL TECHNIQUE

A. Sample Preparation

A model of the sample geometry is shown in Fig. 2(a). The materials were Nb for the superconducting rod,

[19] From (29) we may find that the average value of the superfluid velocity $\langle v\rangle_{\text{av}}$ is proportional to $(1-f^2)^{1/2}$. Thus, the relation between $\langle v\rangle_{\text{av}}$ and H_e may be found from (27). We shall make no use of such a relation in the present discussion.

[20] V. L. Ginzburg, Dokl. Akad. Nauk SSSR 83, 385 (1952).

Al-Al_2O_3 for the nonsuperconducting cylinder, and In for the superconducting cylinder. The transition temperatures (bulk values) for these materials are 9.46°K for Nb, 1.19°K for Al, and 3.407°K for In.[21] Nb rods were obtained from zone-refined Nb, which was made into cylindrical rods in a lathe and then polished with carborundum and aloxite.

The samples were prepared by vacuum evaporation of Al (99.99%) pure) and In (99.999% pure). Films of these materials were condensed on Nb rods, while the rods were rotating at room temperature and a background pressure of $(3–5)\times10^{-5}$ Torr. Two Nb rods were exposed simultaneously to an Al evaporation. The resulting Al films were allowed to oxidize in atmospheric air. Then one of the rods was exposed to an In evaporation. To reduce the partial pressure of oxygen in the system prior to condensing the In film on the rod, In was evaporated over the chamber walls (but not onto the rod).[22] The rod with both Al-Al_2O_3 and In film made up the sample. The rod without In film made up a dummy. The use of the dummy will appear below. Film thicknesses were determined by weighing the rods before and after condensation. For the measurements to be reported below, the thicknesses were 1910±70 Å for the In film and 10 800±500 Å for the Al-Al_2O_3 film. The length of the Nb rod was 40 mm, and its diameter was 1.85±0.01 mm.

B. Electrical Network

The measured quantity was the flux ϕ_J arising from the supercurrent. This flux was measured by a pickup coil surrounding the sample. The presence of the superconduction Nb rod caused the induced voltages to be rather small of the order of a few μV. The detection system for ϕ_J was wide-banded, terminating in a sampling integrator.

The network is shown in Fig. 3. It was a mutual inductance bridge driven at 550 Hz. The detection system had an upper frequency response limit of 10 kHz, which is roughly the 20th harmonic of the drive frequency. The low-temperature part consisted of a liquid-nitrogen-cooled copper solenoide producing the low-frequency field and two pickup coils situated in the liquid helium. The pickup coils were wound on quartz tubes which had a length of 40 mm; the inner diameter was 2.3 mm (slightly greater than that of the Nb rods), and the outer diameter was 3.9 mm. The pickup coils had 500 turns each and these extended 20 mm over the middle part of the quartz tubes. The pickup coils were connected in opposition, but since they were not quite identical, this did not provide the necessary fine balance of the bridge. This was achieved by the variable mutual inductance and the phase compensator as shown in Fig. 3.

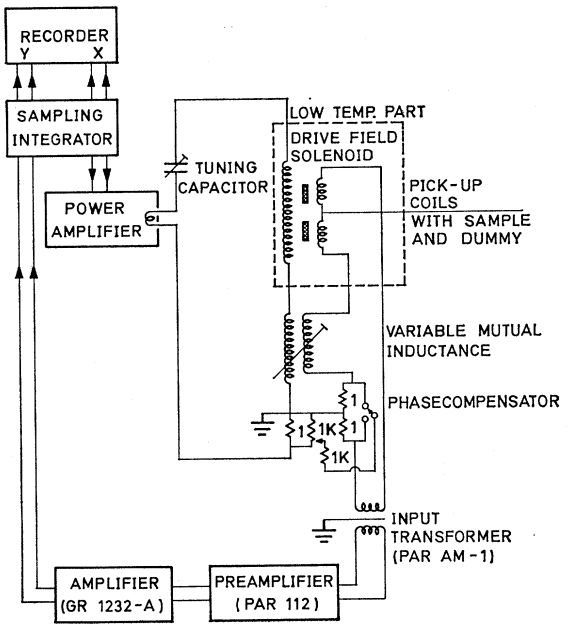

FIG. 3. Diagram of the electrical network.

The sampling integrator had a small "phase window." It supplied the Y sweep of the recorder with the average over roughly 700 periods of an incoming voltage-time waveform at a definite phase. It also supplied the X sweep with a voltage proportional to that phase. As the phase was shifted continously, a period of an incoming voltage-time waveform was traced out in 4 min. The sampling integrator could only be run at the fixed frequency of 550 Hz.

With this bridge, it was possible to balance voltages of the drive frequency only, and because of experimental imperfections (mainly higher harmonics in the drive source), it was necessary to make measurements on empty pickup coils. In these measurements, the bridge was balanced above the expected transition temperature T_c for the sample film (In) to be inserted later on, and voltage-time waveforms were recorded for temperatures below T_c. It was found that the reproducibility of these empty-coil waveforms was better than 20%, and that the lack of reproducibility was due to drift of the bridge balance during the measurements. A possible temperature dependence of the empty-coil waveforms was within the reproducibility. Cycling of the pickup coils from 4.2°K to room temperature did not cause any detectable change in the empty-coil waveforms. Two of the waveforms obtained for empty coils are shown in Fig. 4. The temperatures are above and below T_c, respectively. For comparison, a waveform for sample and dummy inserted is shown.

Temperatures were deduced from the vapor pressure of the liquid-helium bath and controlled by a Cartesian manostate, this giving an accuracy of ±5 m°K.

[21] E. A. Lynton, *Superconductivity* (Wiley-Interscience, Inc., New York, 1962), Chap. 1, p. 5.
[22] Hollis L. Caswell, J. Appl. Phys. 32, 2641 (1961).

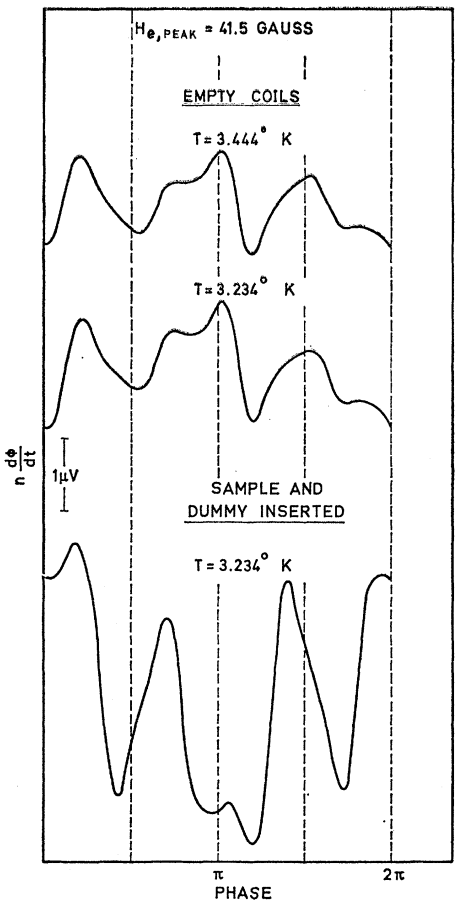

FIG. 4. Voltage-time waveforms for empty coils at $T=3.444$ and 3.234°K, together with waveform at 3.234°K for sample and dummy inserted. Amplitude of external field $H_{e,\text{peak}}=41.5$ G. Transition temperature for sample (In film) was (3.368±0.005)°K. PHASE means the phase of H_e.

C. Experimental Runs

In the experimental runs, the sample was inserted into the one of the two pickup coils and the dummy into the other. To prevent rattling, the ends of the rods were wound with narrow pieces of tape. The bridge was balanced above the expected T_c for the In film. The bath temperature was then lowered (during this, the low-frequency field was turned off) to below T_c and voltage-time waveforms recorded. On raising the bath temperature it was found that above a certain temperature the waveforms were identical to those found for empty coils. This temperature was taken as the transition temperature of the In film.

Each experimental run was performed with a fixed amplitude of the low-frequency field, which was 41.5, 27.6, or 13.8 G. As mentioned above, the low-frequency field was turned off during the transition of the In film to the superconducting state. Thus, this transition took place in the magnetic field of the earth. However, this field is less than 4% of the smallest amplitude used for the external field, and because of experimental inaccuracy (drift of bridge balance), we should not expect to observe any influence of the magnetic field of the earth. This is the reason why, in Sec. II, the fluxoid was assumed to be zero.

Measurements were performed on two In films and also on two Sn films. In the first measurements, we were not aware of the presence of the empty-coil waveforms, and the information obtained was qualitative. The measurements to be reported below were made on a 1910 ±70-Å In film. Prior to and after these measurements, the empty-coil waveforms were carefully measured.

IV. EXPERIMENTAL RESULTS AND DATA TREATMENT

The transition temperature was found to be (3.368 ±0.005)°K, which is 1% lower than that for bulk In.[21] Since transition temperatures of thin films are known to be sensitive to oxygen contamination,[22] stresses,[23] and nearby normal metals,[24] the observed difference from the bulk value is not surprising.

The first part of the data treatment consisted in subtracting the empty-coil waveform from the corresponding waveforms (the same amplitude of the low-frequency field) found with sample and dummy inserted. The results for three temperatures below T_c are shown in the three lower graphs of the left-hand column in Fig. 5. These voltage-time waveforms represent the time derivative of the flux due to the supercurrent multiplied by the number of turns on the surrounding pickup coil. The negative dip appearing (at $T=3.234$ and 3.314°K) before the phase $\frac{1}{2}\pi$ is reached should be noted, since this means a decrease of ϕ_J with increasing external field. The $d\phi_J/dt$ waveforms were integrated numerically to give the flux-versus-phase graphs shown in the middle column. The electrical network allowed the phase (modulo π) of these waveforms relative to that of the external field to be determined with an accuracy of ±3°. Within this limit, no phase shift of ϕ_J relative to H_e was found. This is shown by the upper two graphs in Fig. 5. From the graphs of H_e versus phase and those showing ϕ_J versus phase the ϕ_J-H_e graphs shown at right were obtained.

At the lowest temperature (3.046°K), no deviation from a linear relation between flux and external field was observable. When the temperature was raised towards the transition temperature, a maximum in ϕ_J versus H_e appeared and at the highest temperature (3.314°K) the maximum was followed by a minimum. The presence of the minimum is understandable when it is remembered that the In film is expected to return to the superconducting state when the point $f^2=0$ is passed (cf. Fig. 1). Regarding the hysteresis appearing in these graphs, see Sec. V.

[23] A. M. Toxen, Phys. Rev. **123**, 442 (1961).
[24] P.-G. De Gennes, Rev. Mod. Phys. **36**, 225 (1964).

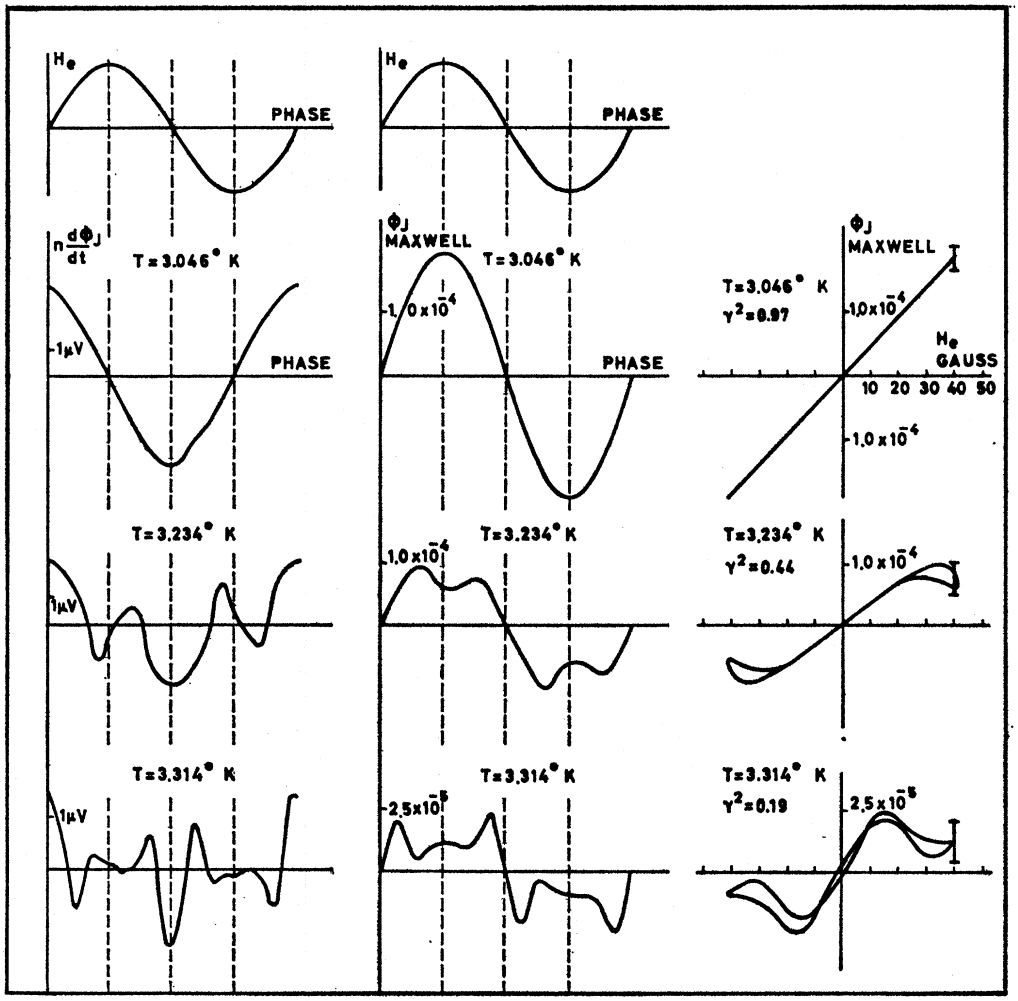

FIG. 5. Experimental results at three temperatures below the transition temperature (3.368±0.005)°K. H_e is the external field; n is the number of turns on pickup coil surrounding sample; ϕ_J is the flux due to supercurrent. Column at left shows the electrically detected voltage-time waveforms corrected for empty coils; these waveforms were integrated numerically to give the waveforms in the middle column, and these in turn were converted to the ϕ_J-H_e graphs shown at right. $H_{e,\text{peak}}=41.5$ G is less than the calculated film critical field at all three temperatures. The values of γ^2 were found from the analysis of these graphs. Vertical arrows are the amplitude of drift of bridge balance. Note expansion of vertical scales on lowest graphs.

The dependence of ϕ_J on H_e displayed in Fig. 5 is in accordance with the qualitative features of the formulas presented in Sec. II. From (30) and (31), we find that the maximum value of $\langle J\rangle_{\text{av}}$, as well as the corresponding value of the external field, decreases when the temperature is raised. Thus, the absence of a maximum in ϕ_J at 3.046°K is interpreted as being due to a too low value of $H_{e,\text{peak}}$. We must mention that 41.5 G was the highest obtainable amplitude of H_e.

For the measurements displayed in Fig. 5, the amplitude of the external field was 41.5 G. Measurements at lower amplitudes (27.6 or 13.8 G) were carried out at each of the experimentally chosen temperatures below T_c. The results for one of these temperatures (3.314°K) are shown in Fig. 6. The graph for the 41.5-G amplitude is the same as that shown in the right-hand lowest corner of Fig. 5. It is seen that the graph for the 27.6-G amplitude repeats the corresponding part for the 41.5-G amplitude. The same was the case for the 13.8-G amplitude. For clarity this is not shown in the figure.

Before we try a quantitative examination of the ϕ_J-H_e graphs, let us summarize the factors which were decisive ones in concluding that these graphs should be interpreted as representing the dependence of J on H_e described in Sec. II. (a) The correction for empty-coil waveforms ensures that the $d\phi_J/dt$ waveforms of Fig. 5 do not originate in the electrical network. As regards the drift of bridge balance, this gave rise to uncertainty in the main frequency voltages only, not in the higher harmonics. (b) The use of a dummy, and the fact that the $d\phi_J/dt$ waveforms disappeared at the transition temperature of the material used for the supercon-

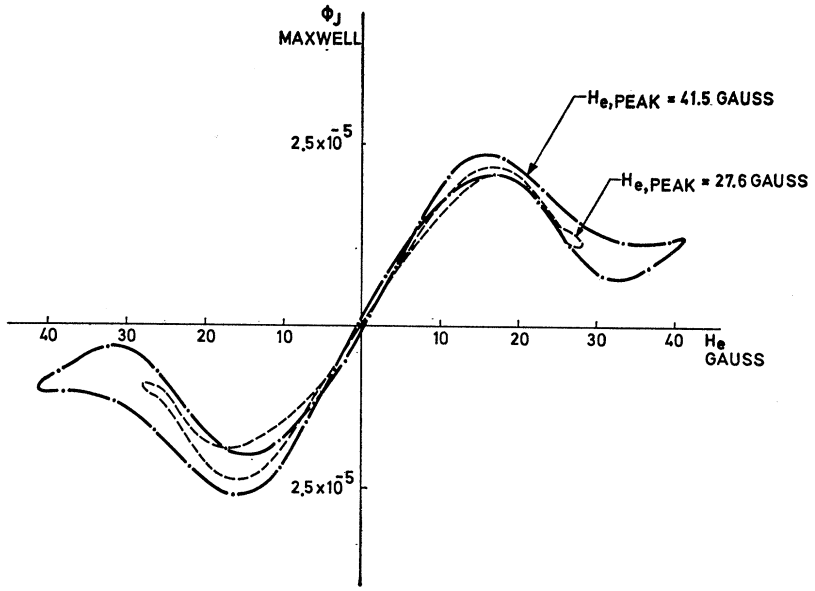

FIG. 6. ϕ_J-H_e graphs at two different field amplitudes $H_{e,\text{peak}}=41.5$ and 27.6 G. $T=3.314$°K.

ducting cylinder (In or Sn), ensures that the $d\phi_J/dt$ waveforms do originate in this cylinder. (c) In the following, we shall see that the temperature dependence and the maximum value of ϕ_J is found—within experimental accuracy—to be in agreement with the predictions of the GL theory.

Below is reported a quantitative examination of the ϕ_J-H_e graphs. This was undertaken in the light of Eqs. (30)–(35) in Sec. II. These equations were applied under the assumption that the observed quantity ϕ_J is related to the average current density by the equation

$$\phi_J=(4\pi d/c)\langle J\rangle_{\text{av}}2\pi r_1(d_1+\tfrac{1}{2}d). \tag{36}$$

The first term on the right-hand side of (36) represents that part of ϕ_J which is in the wall of the nonsuperconducting cylinder, and the second term represents that part of ϕ_J which is in the wall of the superconducting cylinder (cf. Fig. 1). In (36) we have neglected end effects (bending of ϕ_J flux lines at the ends of the sample). This was found to be justified by independent measurements.[25]

For the quantities r_1 and d, we shall use the radius of the Nb rod and the thickness of the In cylinder, respectively. The value of d_1 will appear to be determined from the experimental data. We shall also need the temperature dependence of the penetration depth. This was assumed to be

$$\lambda(t)^2=\lambda(0)^2(1-t^4)^{-1},\quad t=T/T_c. \tag{37}$$

[25] In these measurements, the classical skin effect in a cylindrical metal rod was measured using the same dimensions of a pickup coil as described in Sec. III; the dimensions of the metal rod were also the same as that of the Nb rod used in the present experiment. The skin-effect measurements gave a value of the room-temperature specific resistance of the metal rod which agreed with that found in handbooks.

The reciprocal slope of the ϕ_J-H_e graphs for small H_e is found from (33), (36), and (37):

$$(d\phi_J/dH_e)^{-1}=[2\pi r_1 d_1(1+d/2d_1)]^{-1}+[\pi r_1 d_1(1+d/2d_1)^2\gamma(0)^2]^{-1}(1-t^4)^{-1}, \tag{38}$$

where $\gamma(0)^2=2dd_1/\lambda(0)^2$. Figure 7 shows reciprocal slopes, found from the ϕ_J-H_e graphs, plotted against $(1-t^4)^{-1}$. The two lowest points in Fig. 7 arise from ϕ_J-H_e graphs that are straight lines, while the other

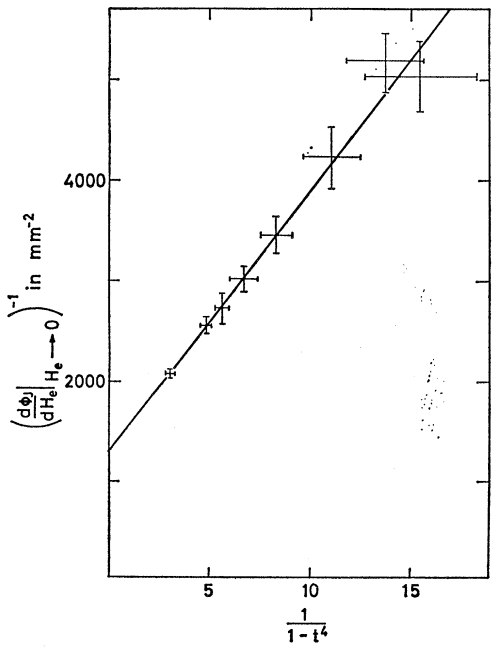

FIG. 7. Reciprocal slope of ϕ_J-H_e graphs for $H_e\to 0$ plotted against $(1-t^4)^{-1}$. $t=T/T_c$.

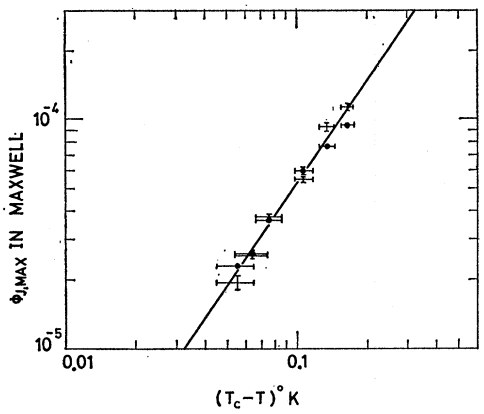

FIG. 8. Maximum values of ϕ_J found from ϕ_J-H_e graphs plotted versus T_c-T. Log-log scale. +, increasing H_e; •, decreasing H_e.

points arise from graphs having a more or less pronounced maximum. It is seen that whatever the ϕ_J-H_e graphs look like, their slopes for small external fields obey a relation of the form given in (38). The vertical intersection and the slope of the straight line drawn through the experimental points in Fig. 7 are found to be

$$[2\pi r_1 d_1(1+d/2d_1)]^{-1}=1270\pm30 \text{ mm}^{-2}$$

and

$$[\pi r_1 d_1(1+d/2d_1)^2\gamma(0)^2]^{-1}=264\pm5 \text{ mm}^{-2}.$$

If we use $2r_1=1.85\pm0.01$ mm and $d=1910\pm70$ Å, then we find that

$$d_1(1+d/2d_1)=1360\pm40 \text{ Å},$$
$$d_1=405\pm75 \text{ Å},$$
$$\gamma(0)^2=2.9\pm0.5,$$
$$\lambda(0)=730\pm40 \text{ Å}.$$

The values of d_1 and $\lambda(0)$ will be discussed in Sec. V.

According to (30) and (36), $\phi_{J,\max}$ has the same temperature dependence as H_{cb}/λ. Assuming that $H_{cb}(t)=H_{cb}(0)(1-t^2)$, and a temperature dependence of λ as given by (37), we find, near T_c, that

$$\phi_{J,\max,\text{theoret}} \propto (T_c-T)^{3/2}. \quad (39)$$

Figure 8 shows the experimentally found values of $\phi_{J,\max}$ plotted against T_c-T on a log-log scale. The slope of the straight line drawn through the experimental points is 1.5 ± 0.1, which gives

$$\phi_{J,\max,\text{expt}} \propto (T_c-T)^{1.5\pm0.1}.$$

In order to compare the magnitude of $\phi_{J,\max}$ with that predicted theoretically, we might insert in (30) the handbook value of H_{cb} and the value of λ found experimentally. However, it was found to be more instructive to calculate H_{cb} from the experimental parameters already found. From (30) and (36) we find that

$$H_{cb}=\phi_{J,\max}\frac{(27/8)^{1/2}\lambda[1+d(1+d/3d_1)/d_1]^{1/2}}{2\pi r_1 d d_1(1+d/2d_1)^2}. \quad (40)$$

The results of the calculation of the right-hand side of (40) are plotted against $1-t^2$ in Fig. 9. The slope of the straight line drawn through the experimental points is

$$H_{cb}(0)=255\pm40 \text{ G}.$$

The handbook value for $H_{cb}(0)$ is 283 G,[21] which means that within experimental accuracy the magnitude of $\phi_{J,\max}$ agrees with that predicted by GL theory.

The GL parameter κ may be calculated from (5) by inserting the experimental values of λ and H_{cb}. For the range of temperatures used in the present experiment we then find that

$$\kappa=0.29\pm0.08.$$

In the calculations of Sec. II we assumed f to be independent of position. This approximation can be made without too great an error as long as d is less than the coherence length ξ, which, according to Gor'kov,[17] is $\xi\approx\lambda/\kappa$. Using the above value of κ, we find that ξ ranges from approximately 4400 Å at 3.046°K to 9900 Å at 3.314°K. Since d was 1910 Å, the requirement $d<\xi$ was fulfilled.

The value of H_e at which the maximum of ϕ_J is predicted to occur, and the value for which ϕ_J is predicted to become zero (after the maximum), was calculated from (31) and (32). The results are shown in Table I.

TABLE I. Characteristic values of H_e.

T (°K)	H_e for $\phi_J=\phi_{J,\max}$ from Fig. 5 (G)	$H_{2/3}$ from Eq. (31) (G)	H_e for $\phi_J=\phi_{J,\min}$ from Fig. 5 (G)	H_0 from Eq. (32) (G)
3.205	37±4	36±12	···	39±11
3.234	31±4	30±10	···	36±11
3.261	27±3	25±9	···	32±10
3.292	21±2	20±8	39±2	26±9
3.304	20±2	18±7	37±3	25±8
3.314	16±2	16±6	34±4	23±8

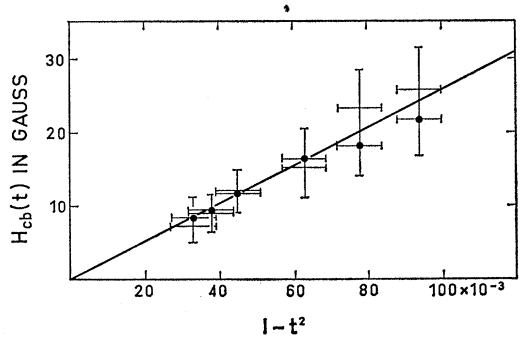

FIG. 9. $H_{cb}(t)$ calculated from (40) and plotted against $1-t^2$. +, increasing H_e; •, decreasing H_e. Slope of straight line gives $H_{cb}(0)=255\pm40$ G.

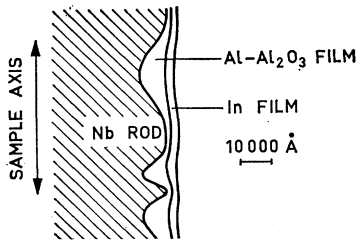

FIG. 10. Supposed qualitative structure of a cross section through the sample surface along the sample axis.

The theoretical values of $H_{2/3}$ should be compared with those for which ϕ_J is a maximum (cf. Fig. 5). From the numbers in Table I, it is seen that the calculated and the experimentally found values agree with each other. The predicted decrease of ϕ_J to zero was not unambiguously observed. However, we might compare the position of the minima in the ϕ_J-H_e graphs with H_0. Such minima only appeared at the three temperatures closest to the transition temperature. The locations (as given in Table I) of these minima were found by averaging the positions of the minima for both branches of the hysteresis curve, and both signs of H_e. From the numbers in Table I we see that these minima occur at larger values of H_e than H_0.

Film critical fields H_c may be calculated from (35), which gives the ratio H_0/H_c. By inserting $d=1910 \pm 70$ Å and $d_1=405\pm 75$ Å we find that

$$H_0/H_c=0.38\pm 0.13,$$

and H_c may then be calculated from the values of H_0 given in Table I by multiplication of these values with 1/0.38. According to this, we should expect H_c to be larger than the amplitude (41.5 G) of the external field —even for the highest temperature at which the quantitative examination was performed (3.314°K).

V. DISCUSSION

In this section we shall discuss the values found for $\lambda(0)$ and d_1 together with the observed hysteresis.

The GL expression for λ is given by (4) and (6):

$$\lambda^2=\lambda_L^2(1+\xi_0/l). \tag{41}$$

For $\lambda_L(0)$ and ξ_0 we use the values[26] 350 and 2600 Å, respectively. We then find for the electronic mean free path l

$$l\approx 770 \text{ Å}.$$

Independent measurements to justify this value were not made.

As mentioned in Sec. II, the theoretical formulas used in this paper are approximate in the sense that series expansions of hyperbolic functions with argument df/λ have been used. At the lowest temperature ($T=3.046$°K), d/λ is 1.50. When this value is inserted into the exact expressions for H_{cb} and for $(d\phi_J/dH_e)^{-1}$ in the limit $H_e\to 0$, we find that the formulas (38) and (40) are accurate to better than 15% in determining $H_{cb}(t)$ and $\lambda(0)$. Exact expressions are given in the Appendix.

The value of d_1 found from the plot in Fig. 7 was 405 ± 75 Å. As mentioned in Sec. III, the thickness of the Al film—as found by weighing the Nb rod before and after condensation of Al—was 10 800 Å, which is orders of magnitude larger than the value found for d_1. The reason for this is not completely understood, but two possibilities are proposed. First, the surface of the Nb rod was not perfectly smooth. Observed in an optical microscope—before condensation of the films—the rod appeared to have grooves as deep as 1 μm running in the plane perpendicular to its axis. After condensation of the In film, no trace of such grooves could be seen. This leads us to suppose that a cross section through the sample surface along the sample axis qualitatively looks like the drawing in Fig. 10. The second possibility is that the pair potential in the superconducting Nb rod will extend to some distance in the Al film,[24] and thus this film might not be normal throughout.

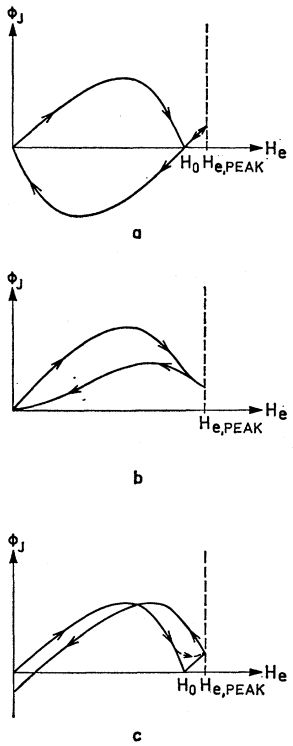

FIG. 11. (a) Expected hysteresis if the fluxoid quantum number changes abruptly at $H_e=H_0$. (b) Hysteresis calculated from graphs like the one in Fig. 11 (a) with a Gaussian distribution of H_0 values centered around $H_{e,\text{peak}}$. (c) Expected hysteresis if the fluxoid quantum number changes gradually in a region around H_0, and ϕ_J in this region jumps from one graph to another which has an appropriate value of the fluxoid quantum number.

[26] A. M. Toxen, Phys. Rev. **127**, 382 (1962).

As mentioned in Sec. III, measurements were performed on three samples besides on the one already described. In these measurements we found transition temperatures of the sample films (In or Sn) which were in accordance with the handbook values. Also, a decrease of ϕ_J as a function of H_e was observed. However, some of the experimental conditions (drift of bridge balance, empty-coil waveforms) were not controlled. For one of the Sn film samples, a quantitative analysis like that in Sec. IV was tried. This sample had 6800 Å Al according to weight, whereas d_1 turned out to be 1400±1500 Å.

As regards the observed hysteresis in the ϕ_J-H_e graphs, we propose that it is due to change of the fluxoid quantum number ν in the region $H_e \approx H_0$. If we assume that ν changes abruptly at $H_e=H_0$, then for H_e larger than H_0 we should expect a hysteresis in the ϕ_J-H_e graphs as shown in Fig. 11(a). Such a kind of hysteresis was never observed, and consequently we shall try to explain why not. First, the value of d/d_1 is probably not constant along the length of the cylinder, and we might try to calculate a ϕ_J-H_e graph from graphs with H_0 distributed around some mean value. An example of the result of such a calculation is shown in Fig. 11(b). The distribution function for H_0 was assumed to be Gaussian, centered around $H_{e,\text{peak}}$, and with a half-width equal to 10% of $H_{e,\text{peak}}$. We note that the resulting ϕ_J does not decrease to zero, and that the largest hysteresis occurs in the region of small H_e. The latter fact is in disagreement with the observations, and therefore we shall propose that ν does not change abruptly at $H_e=H_0$ but rather change gradually in a region around H_0, and that in this region ϕ_J may jump from one graph to another which has an appropriate value of ν. Such a kind of hysteresis is sketched in Fig. 11(c).

VI. CONCLUSION

To summarize, it can be said that for $\phi_J \lesssim \phi_{J,\max}$ the ϕ_J-H_e graphs were found—within experimental accuracy—to be in agreement with the predictions of GL theory. Over the maximum, a decrease of ϕ_J was clearly observed. The hysteresis in the ϕ_J-H_e graphs is proposed to be due to change of fluxoid quantum number in a region around H_0.

ACKNOWLEDGMENTS

The author wishes to thank Professor H. Højgaard Jensen for continuous interest, and is greatly indebted to P. Voetmann Christiansen, who proposed the experiment to be done and gave invaluable theoretical support. B. H. Pettersson constructed the variable mutual inductance and E. T. Sørensen the sampling integrator. For critical reading of the manuscript, the author wishes to thank Dr. R. D. Mattuck.

APPENDIX

In this Appendix we shall write solutions to the GL equations for the geometry displayed in Fig. 2(a). The solutions are exact under the assumptions that f is independent of position, the fluxoid is equal to zero, and $r_1 \gg d$, d_1, and λ.

The expression for the vector potential is [cf. Ref. 15, Eq. (19)]

$$A(r)=C_1 I_1(rf/\lambda)+C_2 K_1(rf/\lambda), \tag{A1}$$

where I and K are the modified Bessel functions of the first kind. The integration constants C_1 and C_2 are determined from the boundary conditions

$$\nabla \times \mathbf{A}=\mathbf{H}_e, \quad \text{for} \quad r=r_1+d \tag{A2}$$

and

$$A/d_1=|\nabla \times \mathbf{A}|, \quad \text{for} \quad r=r_1. \tag{A3}$$

This gives

$$C_1=[K_1(\alpha)+\tfrac{1}{2}s\alpha K_0(\alpha)]H_e\lambda/f\Delta(\alpha,\beta) \tag{A4}$$

and

$$C_2=[\tfrac{1}{2}s\alpha I_0(\alpha)-I_1(\alpha)]H_e\lambda/f\Delta(\alpha,\beta), \tag{A5}$$

where

$$\Delta(\alpha,\beta)=I_0(\beta)[K_1(\alpha)+\tfrac{1}{2}s\alpha K_0(\alpha)] + K_0(\beta)[I_1(\alpha)-\tfrac{1}{2}s\alpha I_0(\alpha)], \tag{A6}$$

$$\alpha=r_1 f/\lambda, \tag{A7}$$

$$\beta=(r_1+d)f/\lambda, \tag{A8}$$

$$s=2d_1/r_1. \tag{A9}$$

By using the series expansions for I and K for large arguments[27] one finds that

$$A(r)=\frac{\phi_0}{2\pi r_1^2}h_e r_1 \frac{\cosh[f(r-r_1)/\lambda]+2(\alpha s)^{-1}\sinh[f(r-r_1)/\lambda]}{\cosh(fd/\lambda)+\tfrac{1}{2}s\alpha\sinh(fd/\lambda)} \tag{A10}$$

[27] Milton Abramowitz and Irene A. Stegun, *Handbook of Mathematical Functions* (Dover Publications, Inc., New York, 1965), p. 377.

and, from (11) and (12),

$$f^2=1-\frac{(\lambda/\kappa r_1)^2 h_e^2}{[\cosh(fd/\lambda)+\frac{1}{2}s\alpha\sinh(fd/\lambda)]^2}\{\tfrac{1}{2}[(\lambda/2df)\sinh(2df/\lambda)+1]$$
$$+(d/d_1\gamma^2f^2)[(\lambda/2df)\sinh(2df/\lambda)-1]+(1/\gamma^2f^2)[\cosh(2df/\lambda)-1]\}. \quad \text{(A11)}$$

The average value of A is found to be

$$\langle A\rangle_{\rm av}=\frac{\phi_0}{2\pi r_1^2}h_e r_1\frac{(\lambda/fd)\sinh(fd/\lambda)+(2/\gamma^2f^2)[\cosh(fd/\lambda)-1]}{\cosh(fd/\lambda)+\frac{1}{2}s\alpha\sinh(fd/\lambda)}. \quad \text{(A12)}$$

Here we have used the abbreviations

$$\phi_0=hc/2e, \quad \text{(A13)}$$

$$h_e=2\pi r_1 d_1 H_e/\phi_0. \quad \text{(A14)}$$

PHYSICAL REVIEW VOLUME 181, NUMBER 2 10 MAY 1969

Flux Creep in Type-II Superconductors

M. R. BEASLEY,* R. LABUSCH,† AND W. W. WEBB
Department of Applied Physics and Laboratory for Atomic and Solid State Physics, Cornell University, Ithaca, New York 14850

(Received 3 January 1969)

We have made measurements of the evanescent decay of the irreversible magnetization induced by magnetic cycling of solid superconducting cylinders in order to elucidate the mechanisms of Anderson's thermally activated flux-creep process. A superconducting quantum interferometer device coupled to the creep specimen by a superconducting flux transformer made possible observations of flux changes with a resolution of one part in 10^9. The general applicability of Anderson's theory of flux creep was confirmed and the results were analyzed to show that: (1) The total flux in the specimen changed logarithmically in time, i.e., $\Delta\phi\propto\ln t/t_0$. (2) The logarithmic creep rate $d\phi/d\ln t$ is proportional to the critical current density J_c and to the cube of the specimen radius. (3) The logarithmic creep rate appears to be only weakly temperature-dependent because a proportionality to T is nearly compensated by the proportionality to J_c, which decreases as T increases. (4) The creep process is a bulk process that is not surface-limited (in this case). (5) Flux enters and leaves the surface in discrete events containing from about one flux quantum up to at least 10^3 flux quanta. (6) On departing from the critical state to a subcritical condition, the creep process tends to remain logarithmic in time, but the rate is decreased exponentially by decreasing T and is decreased extremely rapidly by backing off of the applied field from the critical state. (7) At magnetic fields $H<H_{c1}$ on the initial magnetization curve, no flux creep was observed, but the logarithmic creep rate showed a modest increase above H_{c1} and a broad rise as H approached H_{c2}. The creep process is characterized by a dimension parameter VX consisting of a flux bundle volume V and pinning length X, and by an energy U_0, both of which are supposed to be material-sensitive parameters characteristic of the irreversible processes. These parameters were determined from the experiments. Bundle volumes $V\approx10^{-12}$ cm^3 and energies $U_0\approx1$ eV were found, indicating that groups of fluxoids must be pinned and must move cooperatively. The results are found compatible with a recent model for flux pinning that includes these cooperative effects.

I. INTRODUCTION

BASIC to our present understanding of the remarkable current-carrying capacity and characteristic magnetic hysteresis of hard superconductors are the critical-state model[1,2] and Anderson's[3] theory of flux creep. In the critical-state model the virtually static hysteretic internal field and current distributions are ascribed to the pinning of the fluxoid distribution against the electromagnetic driving forces by material inhomogenieties. The Anderson-Kim[3,4] theory of flux creep describes *dynamic* effects arising from the thermally activated motion of the fluxoids past the pinning barriers and thus generalizes the concept of the critical

* Now at Division of Engineering and Applied Physics, Harvard University, Cambridge, Mass.
† Now at the Institut für Metallphysik, Göttingen, Germany.
[1] C. P. Bean, Phys. Rev. Letters 8, 250 (1962).
[2] Y. B. Kim, C. F. Hempstead, and A. R. Strnad, Phys. Rev. 129, 528 (1963).
[3] P. W. Anderson, Phys. Rev. Letters 9, 309 (1962).
[4] P. W. Anderson and Y. B. Kim, Rev. Mod. Phys. 36, 39 (1964).